scientific reports

Check for updates

OPEN

A tunable narrow single-mode bandpass filter using graphene nanoribbons for THz applications

Ghader Mohammadi, Ali Asghar Orouji✉ & Mohammad Danaie

This paper presents a tunable, single-mode narrowband optical filter designed for terahertz applications utilizing graphene nanoribbons. To attain optimal conditions, the filter was devised in three steps. It is composed of two input and output waveguides and a T-shaped resonator with nanoscale dimensions. The transmission spectrum analysis employs the three-dimensional finite difference time domain and coupled mode theory methods. Tunability is achieved through the adjustment of the nanoribbon size and the chemical potential of graphene. The filter demonstrates remarkable performance metrics, including a maximum transmission spectrum efficiency of 99%, a full width at half maximum (FWHM) of 0.115 THz, a quality factor (Q-factor) of 100, and a free spectral range (FSR) of 45 THz. The presented structure holds significant promise for integrated optical components and compact optical devices, showcasing its applicability in the terahertz frequency range. Furthermore, the inherent sensitivity of this structure to changes in the refractive index of the substrate positions it as a potential sensor.

Keywords Bandpass filter, Chemical potential, Graphene nanoribbon, Plasmonics, Tunability

In recent decades, remarkable progress in optical devices has sparked a significant revolution in optical communication[1]. This evolution has resulted in achieving a high-speed, low-loss, high-performance, high-bandwidth, and reliable optical communication network, thanks to substantial advancements in optical technology[2]. Due to the escalating volume of information and the persistent need for high-speed data transmission, along with varied applications in optical communication, there is a clear recognition of the necessity for devices capable of precisely controlling and improving efficiency in the terahertz (THz) frequency. The THz frequency range has garnered considerable interest in recent times due to its potential applications in the fields of biology, medicine, imaging, sensing, and telecommunications[3].

In the THz spectrum, researchers have shifted their focus to graphene as a highly promising nanomaterial, given its exceptional electronic, optical, and mechanical characteristics. Graphene, a two-dimensional crystal of carbon atoms with a single-atom thickness, forms a honeycomb lattice due to the strong covalent bonds between each carbon atom, facilitated by its three valence electrons[4]. The distinctive properties of graphene in the THz range, coupled with its ability to manipulate optical parameters, position graphene optical devices as potent tools in the field of optoelectronics[5]. In recent years, significant advancements have been made in the study of surface plasmon polaritons (SPPs) in graphene, surpassing developments in noble metals such as gold and silver. This progress is driven by the distinctive electrical and optical properties of graphene, its tunability, reduced losses, sustained collective excitation, and effective light confinement[6]. SPPs on graphene represent coherent electron oscillations occurring at the interface between graphene and dielectric materials[7]. In addition, graphene has the ability to support guided GPPs in both transverse electric (TE) and transverse magnetic (TM) modes, ranging from mid-infrared frequencies to the THz range. A multitude of devices utilizing graphene have been extensively designed and researched to date, encompassing a range of applications such as fibers[8], filters[9], absorbers[10], sensors[11], modulator[12], and more.

One essential component in signal processing, optical filters selectively allow the transmission of light at specific wavelengths while effectively eliminating unwanted components[13]. Tunable optical filters based on graphene in the THz band represent an advanced focus within the realms of nanoelectronics and nanophononics. The band structure and band gap can be modified by adding impurities and applying electric and magnetic fields[14]. In addition, the optical characteristics are controlled by the surface conductivity of graphene, which is a function of the chemical potential. Adjusting the chemical potential of graphene and changing the Fermi energy level affects the absorption coefficient of graphene for light waves, allowing light to be manipulated and controlled in optical

Faculty of Electrical and Computer Engineering, Semnan University, Semnan, Iran. ✉email: aliaorouji@semnan.ac.ir

filters[15]. In general, the chemical potential of graphene is altered by applying electric voltage, chemical doping, and electromagnetic fields. This allows the frequency of graphene filters to be adjusted according to the application after the manufacturing process[16]. Graphene optical filters serve as advanced high-speed optoelectronic and telecommunication devices. Leveraging the nanoscale dimensions and distinctive properties of graphene, these filters outperform conventional counterparts in terms of performance and efficiency. To date, a variety of graphene optical filters have been developed and introduced for applications in the THz region. These filters leverage graphene's notable attributes, including a high transmission coefficient due to its real refractive index and a relatively favorable absorption coefficient due to its imaginary refractive index[17].

In recent years, there has been the notable emphasis on filters fabricated from graphene nanoribbons (GNRs), which constitute a subset of optical graphene filters. GNR configurations support both edge mode and waveguide propagation. When the width of a GNR is on the order of tens of nanometers (nm), only the edge mode is present. The presence of the edge mode significantly enhances the filtering capabilities of GNRs, influenced by quantum confinement, edge structures, and lattice characteristics. The fabrication process for GNRs represents a significant milestone in technological development. In the domain of nanoscale optical devices, achieving GNRs with precisely controlled band gaps is crucial, and various methods, including electron beam lithography, are employed for their production[18]. Combining graphene with noble metals is another method for designing tunable graphene filters. Theoretical and experimental investigations have demonstrated the capability of surface plasmon polaritons (SPPs) to propagate along the surfaces of graphene and thin metal layers. Scientists have theorized that carrier mobility can effectively modulate SPPs in plasmonic graphene. Plasmonic graphene has emerged as a promising avenue in the realm of nanoscale optical filters. Integrating graphene with plasmonics using noble metals such as silver offers dual benefits: enhancing graphene's optical properties through plasmonic nanostructures and utilizing graphene to manipulate the optical response of nanoscale plasmonic arrays[19]. Another category of graphene filters involves the use of dielectrics to guide emission modes, combined with graphene tape as a controllable absorber to selectively filter portions of the transmission spectrum within waveguides or resonators. In this approach, the optical switching functionality of the filter depends on the transmission spectrum passing through the dielectric and undergoing electrochemical absorption. By manipulating the graphene to achieve high or low loss states, the resonant mode can be either suppressed or activated, enabling dynamic adjustment of the filter's performance[20]. Filters that integrate a combination of a graphene waveguide for transmitting the spectrum and GNRs for filtering and absorbing specific segments of the transmission spectrum represent another category of graphene filters. An alternative method for designing adjustable graphene filters involves the utilization of GNRs on a graphene waveguide with a dielectric substrate. The filter design for selecting the transmission spectrum is facilitated by employing two distinct chemical potentials for the waveguide. GNRs exhibit a band structure analogous to that of narrow dielectric waveguides and plasmonic nanowires, where emissive modes are coupled with higher energy. In contrast to thicker plasmonic waveguides utilizing noble metals, plasmons propagating in graphene ribbons demonstrate a concentrated electric field near the edges and along the graphene ribbon. The dispersion relation of these plasmons can be tailored by adjusting the spacing and relative configuration of nanoribbons in a pair[21]. The final method explored in this study involves the use of filters composed of multiple alternating dielectric layers and graphene layers to transmit specific portions of the spectrum. This approach employs one-dimensional non-periodic photonic crystals integrated with graphene. Dielectric plates arranged in a non-periodic sequence are interspersed with graphene sheets positioned at the interfaces of adjacent dielectric layers. The resulting photonic contour crystals exhibit fractal structures, supporting discrete resonance channels within the transmission spectrum. This configuration enables the realization of dual channels and multi-filter functionalities within hybrid systems. The central wavelength and transmission characteristics of each channel can be modulated by adjusting the chemical potential of graphene and the incident angle. Moreover, multiple channels can be selectively activated or deactivated through control of the chemical potential of graphene[22]. One of the primary applications of single-mode narrowband graphene filters is in sensing and detection. With a sufficiently narrow transmission spectrum, these filters enhance sensor sensitivity, enabling the accurate measurement of gases, chemicals, and biological substances. Furthermore, graphene filters enable precise terahertz imaging, which is valuable for security investigations, medical diagnostics, and optical telecommunication receivers, where they facilitate optimal frequency selection[23].

Several challenges associated with graphene filters include achieving high transmission efficiency, a high-quality factor (Q-factor), elimination of signal harmonics, and precise frequency adjustment for applications in telecommunications, imaging, and measurement. In this study, we propose a solution through the design of a novel graphene optical bandpass filter that achieves maximum transmission efficiency while maintaining a relatively high Q-factor, enabling the transmission of a single-mode signal. The filter's frequency can be adjusted by manipulating the chemical potential and optimizing parameters such as L_2, L_5, and Gap. This approach offers a viable means to address specific challenges within this scientific domain.

Model and theory

Utilizing Maxwell's equations for the numerical simulation of electromagnetic wave propagation on the surface of graphene, the permittivity of a GNR is derived from the following Eq. (1)[24].

$$\varepsilon_g = 1 + i\frac{\sigma \eta_0}{k_0 d_g} \tag{1}$$

In the provided Eq. (1), the variable 'i' denotes the imaginary component. Additionally,η_0, k_0, and d_g correspond to the impedance of vacuum, wave vector in vacuum, and thickness of the GNR, respectively. In graphene, the absence of a band gap between the valence and conduction bands confers conductive properties, facilitating extensive interactions of light with a broad range of electromagnetic waves. Employing the surface conductivity

of graphene allows for a comprehensive characterization of its electrical, optical, and magnetic attributes in the plasmonic mode. Consequently, graphene serves as an illustrative model for analyzing graphene-based filters. In this study, GNRs are characterized by surface conductivity, establishing a correlation between surface current and the tangential electric field. The complex surface conductivity of graphene is derived from equations, as delineated below[25].

$$\sigma_{\text{intera}} = 2\frac{e^2 K_B T}{\pi\hbar^2}\cdot\frac{i}{\omega + i\tau^{-1}}\left[\ln\left[2\cosh\left(\frac{\mu_c}{K_B T}\right)\right]\right] \tag{2}$$

$$\sigma_{\text{inter}} = \frac{e^2}{4\hbar}\left[\frac{sinh\left(\frac{\hbar\omega}{2TK_B}\right)}{cosh\left(\frac{\hbar\omega}{2TK_B}\right) + \cosh\left(\frac{\mu_c}{TK_B}\right)} - \frac{i}{\pi 2} ln\frac{(\hbar\omega + 2\mu_c)^2}{(\hbar\omega - 2\mu_c)^2 + (2TK_B)^2}\right] \tag{3}$$

In the equations mentioned above, the symbols K_B, ħ, ω, T, μ_c, and τ represent Boltzmann's constant, reduced Planck's constant, angular frequency, ambient temperature, chemical potential, and relaxation time, respectively. In the THz band, the interband transition is dominant and the optical properties of graphene are similar to metals[26].

According to Fig. 1a, variations in the chemical potential of graphene beyond a frequency of 10 THz exhibit minimal impact on the real component of graphene's surface conductivity. However, as illustrated in Fig. 1b, alterations in the chemical potential induce modifications in the imaginary component of graphene's surface conductivity, predominantly observed at frequencies below 15 THz. Consequently, within the frequency range depicted in Fig. 1, the frequency response of graphene is primarily governed by the imaginary part of its surface conductivity.

One of the principal factors influencing graphene conductivity is the chemical potential, motivating an in-depth exploration of its characteristics. To investigate the chemical potential of graphene, an electric field is applied, inducing electrical doping in the material[27]. Consequently, this process leads to the displacement of Fermi levels relative to the Dirac point, facilitating precise control over the band gap in graphene. The parameter defining the displacement of Fermi levels denoted as the chemical potential (μ_c), assumes a crucial role in this context. By applying an external electric field, the chemical potential can be finely tuned within a broad range (− 1 to 1 eV). This implies that the applied electrical voltage can be directly regulated by the chemical potential of graphene. The approximate relationship between electric voltage and chemical potential is expressed as follows[28]:

$$E_f = \mu_c = \hbar\cdot v_f\sqrt{\frac{\pi\varepsilon_0\varepsilon_r V_{bias}}{e\cdot t}} \tag{4}$$

In the above Eq. (4), v_f, ε_0, ε_r, V_{bias}, and t represent Fermi velocity, air permittivity, substrate permittivity, bias voltage, and substrate thickness, respectively. Furthermore, the chemical potential can be altered through chemical doping. An additional noteworthy technique for inducing a band gap involves the placement of graphene on a substrate.

When graphene is situated on a substrate, the application of an external electric field facilitates the adjustment of charge carriers within graphene. As a result, the Fermi levels can be shifted relative to the Dirac point, as described by the following Eq. (5)[29]:

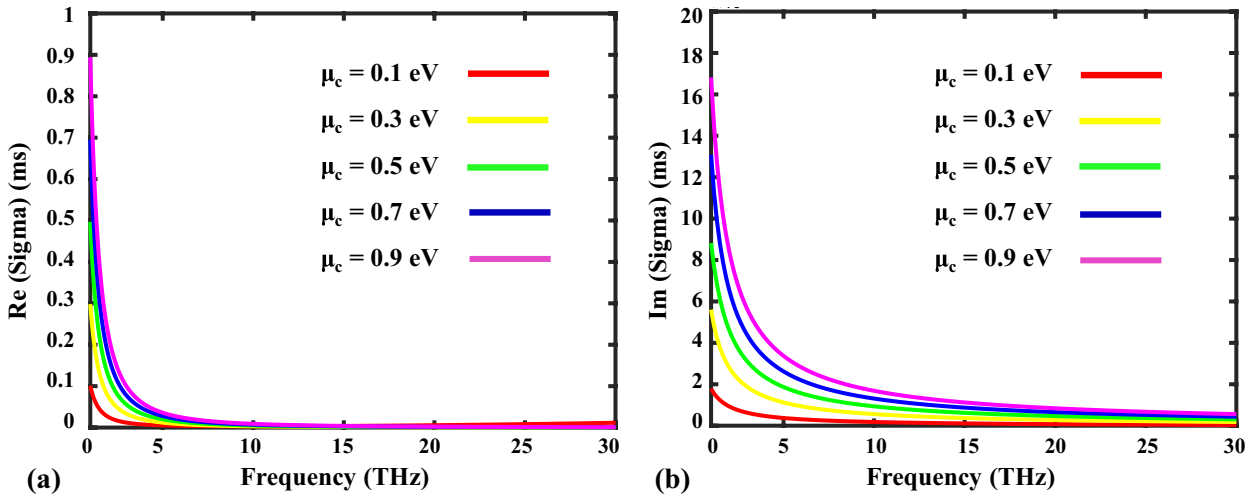

Fig. 1. Surface conductivity of graphene complex for varied chemical potentials (**a**) Real part, and (**b**) Imaginary part.

$$n_s = \frac{2}{\pi \hbar^2 v_f^2} \int_0^\infty \varepsilon [f_d(\varepsilon - \mu_c) - f_d(\varepsilon + \mu_c)] d\varepsilon \quad (5)$$

In the given Eq. (5), n_s represents the charge carrier density on the GNR, and the Fermi distribution function is obtained from $f_d(\varepsilon) = 1/(1 + \exp[(\varepsilon\text{-}\mu_c)/K_B.T])$. Additionally, the mobility of charge carriers in graphene is regulated by the Fermi velocity Consequently, the substrate's presence has the potential to modulate the mobility of charge carriers, thereby influencing the Fermi velocity in graphene[30].

Optical bandpass filter based on graphene nanoribbons

In this study, we employ GNRs to devise an optical tunable bandpass filter aimed at achieving narrowband filtering characterized by high transmission efficiency and single-mode operation. The design comprises three distinct sections featuring various resonators. Each proposed filter configuration encompasses an input waveguide, a specifically contoured resonator, and an output waveguide. GNRs are positioned atop a silica substrate with a refractive index of 1.6 and a silicon layer with a refractive index of 3.44. A gold layer facilitates the application of bias voltage to the graphene. The SiO_2 layer has a thickness of 100 nm, while the Si and Au layers are each 50 nm thick. A modal light source is introduced at the beginning of the left waveguide, with monitoring conducted at the end of the right waveguide along the x-normal direction. Spatial discretization is achieved with a mesh resolution set to 2 nm in both the x and y directions and 2.5 nm in the z direction. The simulation duration spans 10 picoseconds. Numerical simulations are performed using the three-dimensional finite difference time domain (3D-FDTD) method, complemented by perfectly matched layer boundary conditions. The analysis of the filter's transmission spectrum is conducted over the frequency range from 5 to 50 THz.

Design of an optical filter Utilizing a plus-shaped resonator

Figure 2a depicts the schematic of an optical filter featuring GNRs and a plus-shaped resonator. The relevant filter parameters are detailed in Table 1. Figure 2b presents the transmission spectrum of the filter spanning from 5 to 50 THz. Notably, the transmission spectrum exhibits a low efficiency of 26% at a frequency of 24 THz, along with additional modes observed at frequencies of 40 and 47 THz. To reduce the additional harmonics, a gap was introduced between the input waveguide, the resonator, and the output waveguide. Figure 2c,d illustrate the magnitude distribution of the electromagnetic field at frequencies of 24 and 47 THz, respectively. The dashed line delineates the magnitude of the electromagnetic field distribution. To enhance the efficiency of the transmission spectrum and mitigate the presence of additional modes, the utilization of an E-shaped resonator is proposed in the subsequent section.

Design of an optical filter utilizing an E-shaped resonator

To achieve a single-mode spectrum with a narrow bandwidth and eliminate additional harmonics, we widened the gap between waveguides to 50 nm. We incorporated two GNRs of length L_5, each measuring 160 nm, on both sides of the L_4 GNR. The resonator shape was configured as two E joined together. The specifications of the filter are detailed in Table 2.

The two-dimensional schematic of the second proposed filter is illustrated in Fig. 3a. The transmission spectrum, depicted in Fig. 3b, demonstrates the complete removal of additional harmonics within the 5–50 THz range, resulting in a single-mode signal over a wide frequency range. Figure 3c,d present the field distribution size from the y–x and y–z views at a frequency of 15 THz, respectively. As evident from Fig. 3, the efficiency of the filter's frequency response is suboptimal. Modifications have been implemented in the resonator and waveguides to increase the efficiency of the transmission spectrum, as detailed in the following section.

Tunable narrow single-mode bandpass filter

In the third proposed filter, as illustrated in Fig. 4a, we introduced modifications to the second proposed filter aimed at maximizing the efficiency of the transmission spectrum while preserving a narrow single-mode signal. Specifically, L_3 GNRs were removed in Fig. 3a, and L_3 GNRs with a size of 40 nm were added to the terminus of L_4 GNRs. The filter resonator adopted a T-shaped configuration. The filter specifications are outlined in Table 3. Figure 4b illustrates the three-dimensional schematic of the filter, depicting the utilized substrates.

The results of the simulation using FDTD, described in Fig. 4c, demonstrate a peak efficiency of 99% with a Q-factor of 100, a FWHM (full-width at half-maximum) of 0.115 THz, and a free spectral range (FSR) of 45 THz. The transmission spectrum of the proposed filter in Fig. 4a can be calculated using coupled mode theory (CMT). In CMT, a structure is analyzed based on the coupling between two waveguides or a resonator. Equation (6) provides the transfer function[31].

$$t_f = \frac{\frac{1}{Q_\omega}}{2\delta j + \frac{1}{Q_i} + \frac{1}{Q_\omega}} \quad (6)$$

In the above Eq. (6), Q_w is the Q-factor due to coupling waveguide losses and Q_i is the Q-factor due to intrinsic losses. $\delta = \frac{f - f_0}{f_0}$ is used to normalize the frequency, where f_0 is the resonance frequency of the filter[32]. For the proposed filter in Fig. 4a, Q_w and Q_i are found to be 90 and 17,550, respectively In Fig. 4d, the dashed red curve shows the transmission spectrum obtained using the CMT method, and the solid blue curve shows the 3D-FDTD simulation results. We observe that the results of FDTD and CMT methods are almost aligned.

Figure 5a shows the magnitude of the magnetic field distribution at the resonance frequency, while Fig. 5b illustrates the magnitude of the magnetic field distribution at the cutoff frequency, both from the x–y view.

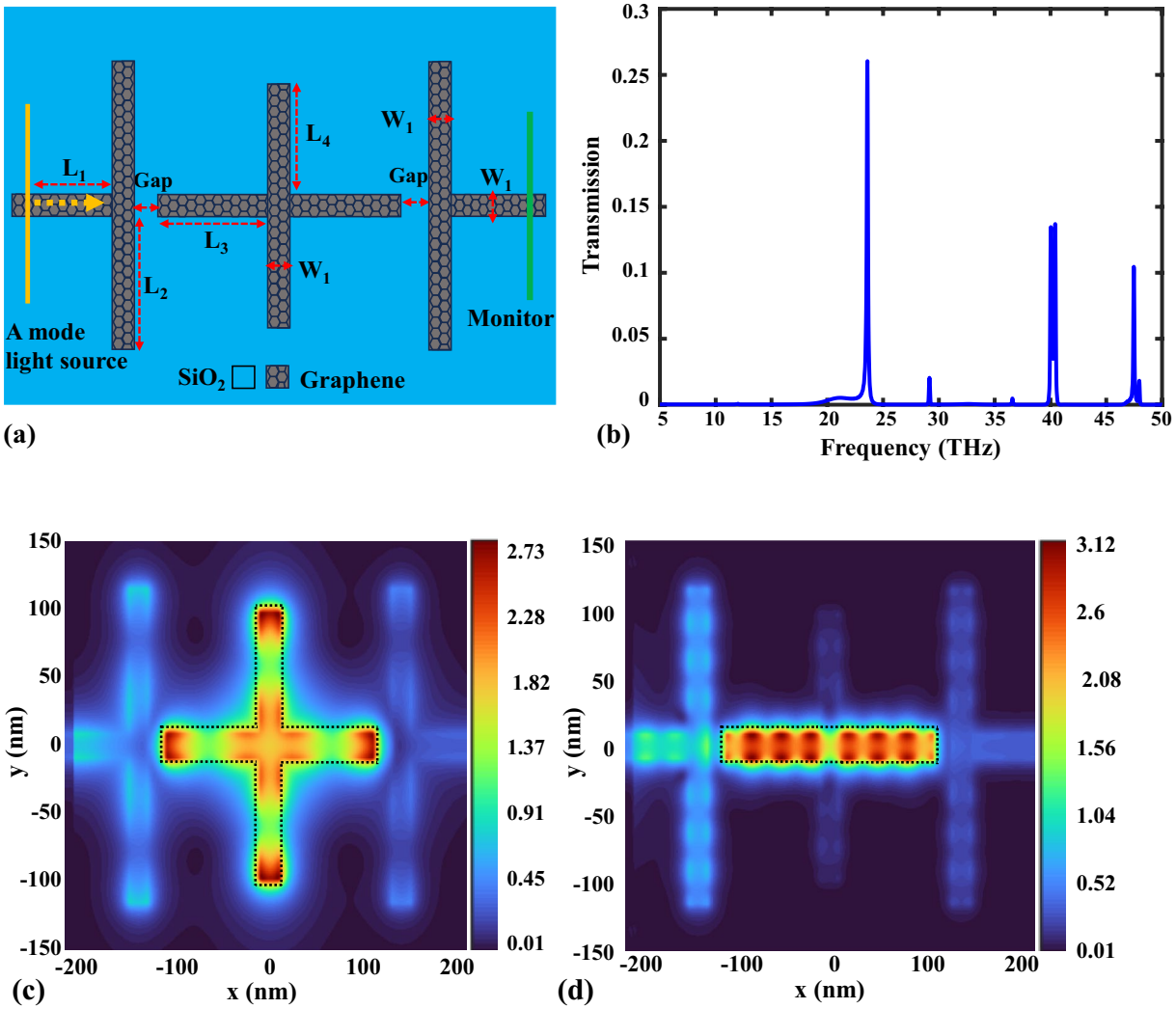

Fig. 2. The first proposed filter: (**a**) Two-dimensional schematic of the structure. (**b**) transmission spectrum in the range of 5–50 THz. (**c**) Magnitude of field distribution at frequency 24 THz. (**d**) and frequency 47 THz.

Parameter	L_1	L_2	L_3	L_4	W_1	Gap
Value (nm)	60	120	100	100	20	20

Table 1. Parameters for optical filter featuring a plus-shaped resonator.

Parameter	L_1	L_2	L_3	L_4	L_5	W_1	Gap
Value (nm)	60	120	70	100	160	20	50

Table 2. Parameters for optical filter featuring an E-shaped resonator.

Figure 5c,d depict the magnitude of the magnetic field distribution at the resonance frequency of 11.5 THz from the z–x view and the y–z view, respectively. The frequency response of the optical filter designed with GNRs, can be adjusted through various methods. These include altering the length and width of GNRs, introducing a gap between the resonator and the input/output waveguides, and modifying the substrate's refractive index to attain an optimal filter configuration. Moreover, resonance frequencies can be easily manipulated by tuning the chemical potential of graphene, enabling the creation of an electrically tunable bandpass filter without requiring changes to the structural parameters.

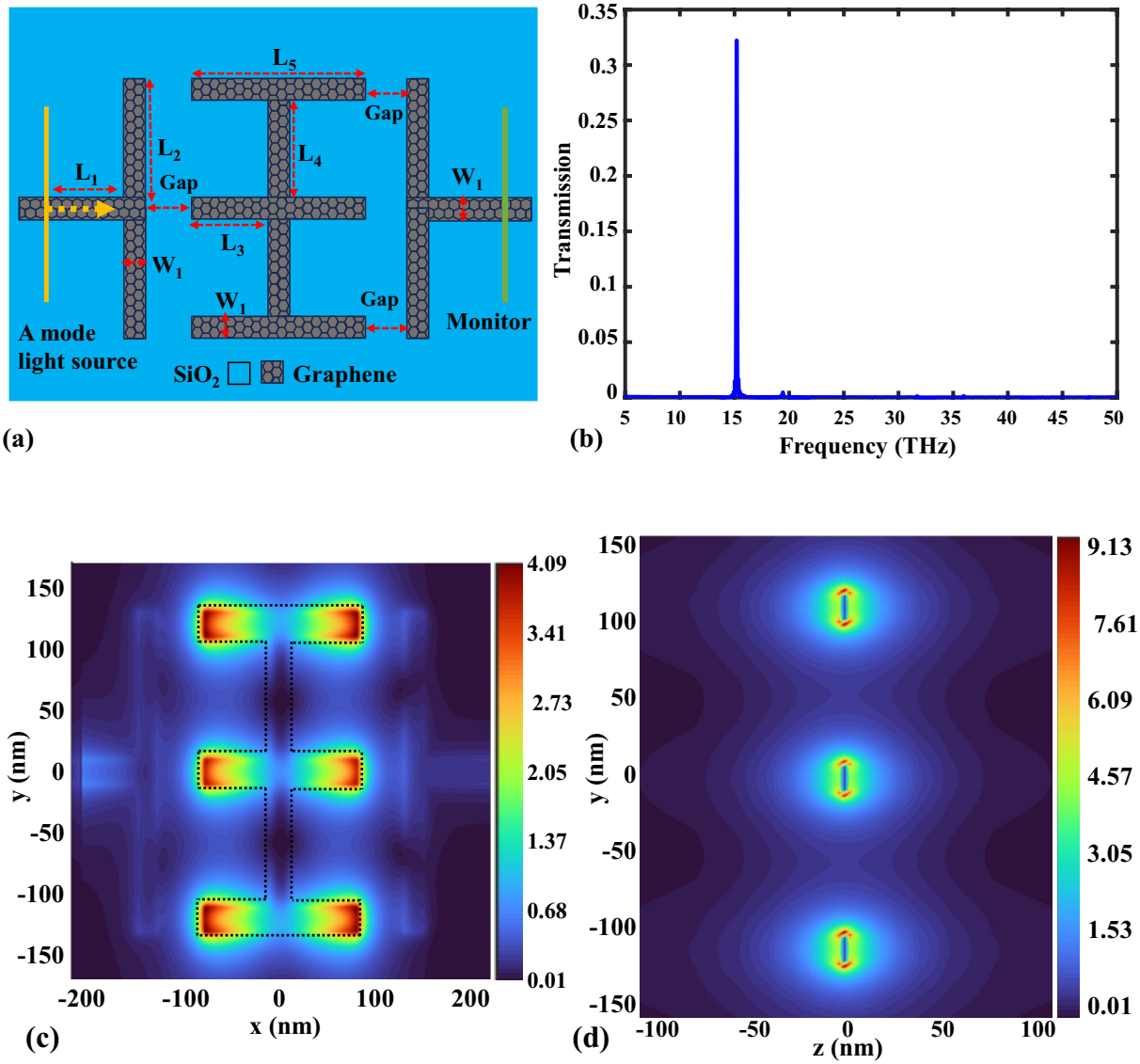

Fig. 3. The second proposed filter: (**a**) Two-dimensional schematic of the structure. (**b**) transmission spectrum in the range of 5–50 THz. (**c**) Magnitude of field distribution at 15 THz from y–x view, (**d**) from y–z view.

Possibilities of the measurement setup

According to Fig. 6, we use a THz pump laser, lenses, couplers, polarizers, and a terahertz optical detector to setup the filter measurement. A THz broadband wave in the range of 5–50 THz is produced by the THz pump laser[33]. The wave then passes through the lens and polarized lens, which is adjusted according to the test conditions and coupled to the graphene filter by an input coupler. At the end of the filter output waveguide, an output coupler, polarizer, and lens direct the wave to the THz optical detector for the necessary analysis and measurement[34]. In such structures, the top gate method is used to adjust the chemical potential. Ion gel layers, typically consisting of a solid electrolyte in a polymer solution containing soft ions, are placed on GNRs[35]. Ion gels can be used to apply a high electric field to graphene, enabling electrostatic doping. This allows the carrier density in graphene to be controlled by the voltage applied through the ion gel. The ionic gel forms a capacitive pair with the graphene, facilitating efficient voltage application without direct electrical contact. Additionally, ionic gels are flexible and can conform to irregular surfaces, making them suitable for flexible electronic devices incorporating graphene[36].

The choice of ionic gel depends on factors such as ionic conductivity, mechanical properties, stability, and compatibility with graphene[37]. The most important ionic gels for applying voltage to graphene are polyvinylidene fluoride-co-hexafluoropropylene (PVDF-HFP)[38] and ethylene oxide[39] with ionic liquid inclusion, as they possess high ionic conductivity and stability. To examine the effect of these ionic gels on the simulation results, we placed the ionic gels as a dielectric on top of the filter, repeated the simulation with different thicknesses, and then compared the results. Figure 7 shows the filter simulation results with ion gel thicknesses of 80, 100, 120, and 140 nm. The blue curve represents the transmission spectrum of the filter without the ion gel layer. Figure 7a shows the frequency response of the filter with ethylene oxide ion gel (refractive index of 1.359), while Fig. 7b shows the

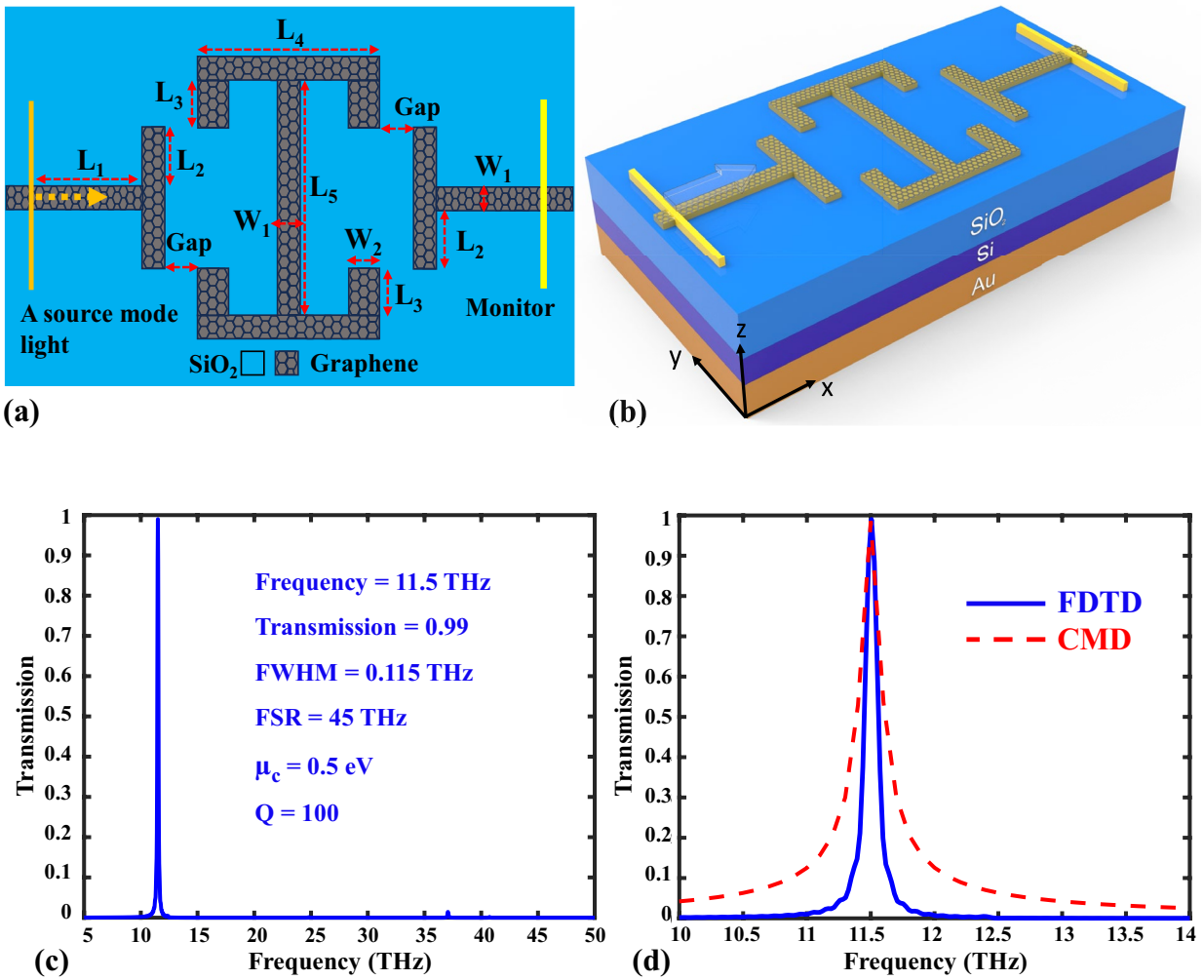

Fig. 4. The third proposed filter: (**a**) Two-dimensional schematic of the structure. (**b**) Three-dimensional schematic of the filter with the substrate. (**c**) Transmission spectrum in the range of 5–50 THz. (**d**) The transmission spectrum obtained by numerical FDTD (solid blue line) and theoretical CMT (dashed red line) methods in the range of 10–14 THz.

Parameter	L_1	L_2	L_3	L_4	L_5	W_1	W_2	Gap
Value (nm)	120	50	40	160	200	20	30	30

Table 3. Parameters for tunable narrow single-mode bandpass filter.

response with PVDF-HFP ion gel (refractive index of 1.42). It can be observed that introducing the ionic gel causes a shift in the resonant frequency of the filter and a slight decrease in the transmission spectrum's efficiency.

In Fig. 8a, the filter transmission spectrum's efficiency is compared for ion gel thicknesses ranging from 80 to 140 nm. It can be observed that as the ion gel thickness increases from 80 nm, the efficiency of the transmission spectrum decreases. The most optimal thickness is found to be 80 nm for both ethylene oxide and PVDF-HFP ionic gels, with a decrease in efficiency of 1% and 2%, respectively, compared to the structure without an ionic gel. In Fig. 8b, the filter frequency is compared for ion gel thicknesses ranging from 80 to 140 nm. A frequency shift is observed compared to the structure without an ion gel. To achieve the best possible performance without significantly affecting the filter transfer efficiency, an 80 nm ion gel thickness is chosen, resulting in a negligible impact on the filter transfer efficiency. In this case, we observe a frequency shift of 1 THz and 1.2 THz for the ethylene oxide and PVDF-HFP ionic gels, respectively.

Results and discussions

Analyzing the filter's frequency response by varying the chemical potential

Under normal conditions, graphene exhibits a zero-band gap. To achieve optimal waveguide profiles in graphene sheets and nanoribbons, adjustments to the chemical potential and Fermi energy levels can be made by applying

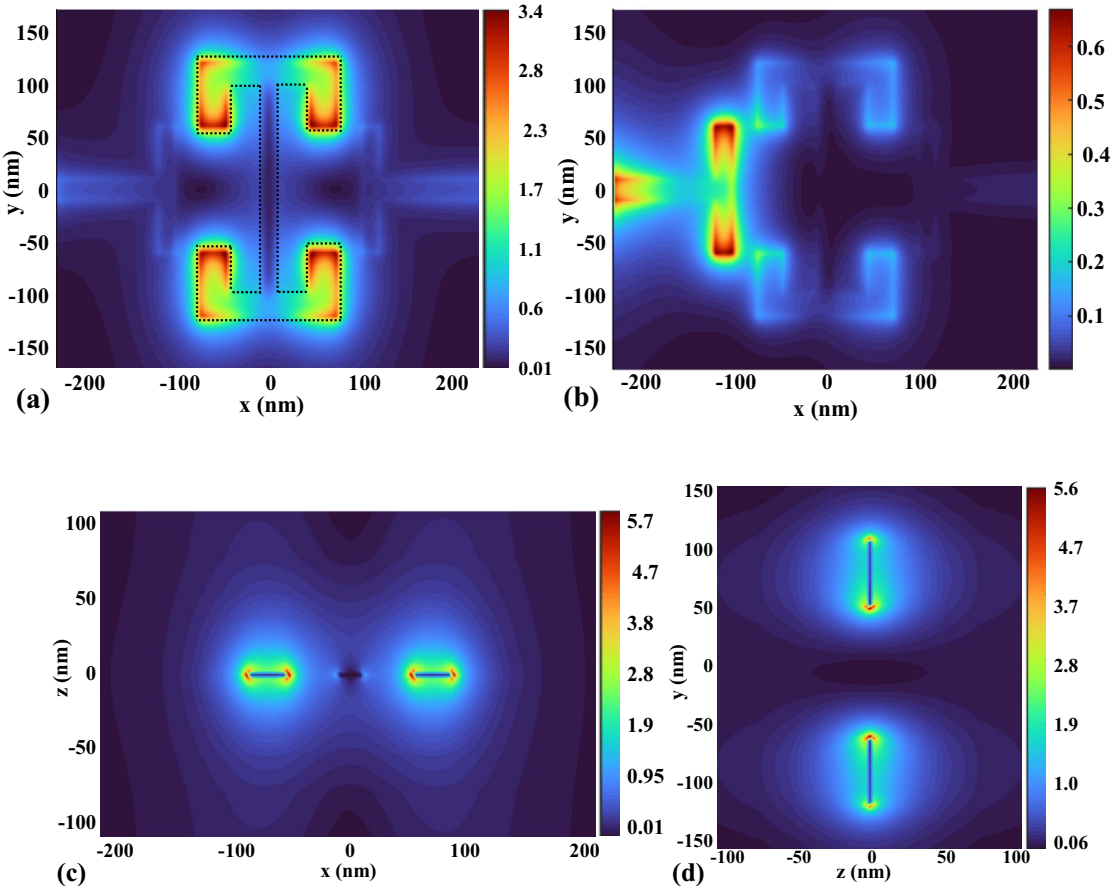

Fig. 5. Magnitude of field distribution from y–x view. (**a**) At the pass frequency of 11.5 THz, and (**b**) at the cutoff frequency of 10.5 THz; (**c**) from z–x view; (**d**) from y–z view.

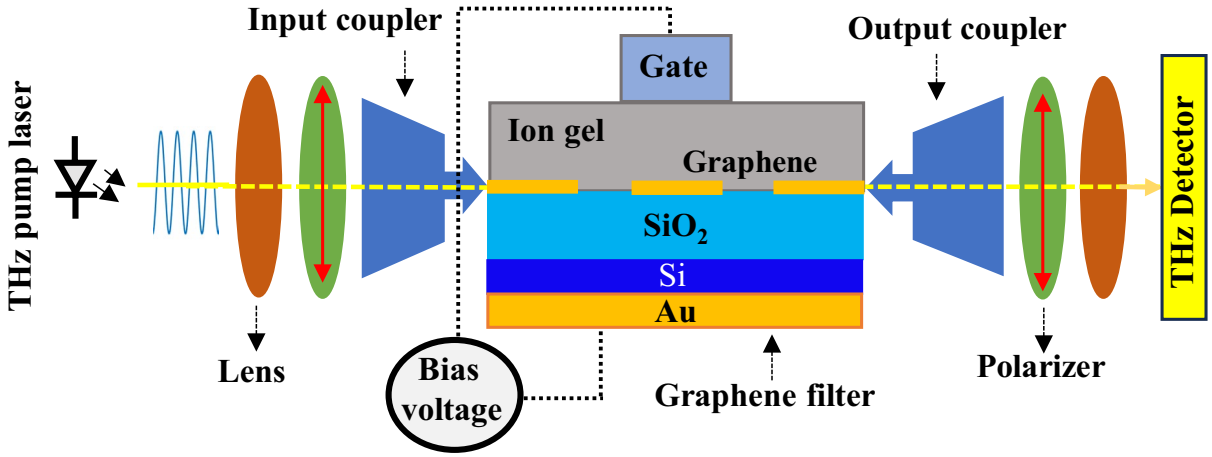

Fig. 6. Schematic of the measurement setup and adjusting the chemical potential of the filter.

a gate voltage (bias voltage)[40]. Consequently, the surface conductivity of graphene and the transmission spectrum of the filter are altered. This remarkable property allows for post-manufacturing modification of the filter's frequency response to suit various applications by applying gate voltage. Figure 9a illustrates the frequency response of the filter to variations in the chemical potential of graphene. To calculate the gate voltage for graphene, we first determine the substrate capacitance using the following Eq. (7)[41]:

$$C_{0x} = \frac{1}{\frac{1}{C_{sio2}} + \frac{1}{C_{si}}} \tag{7}$$

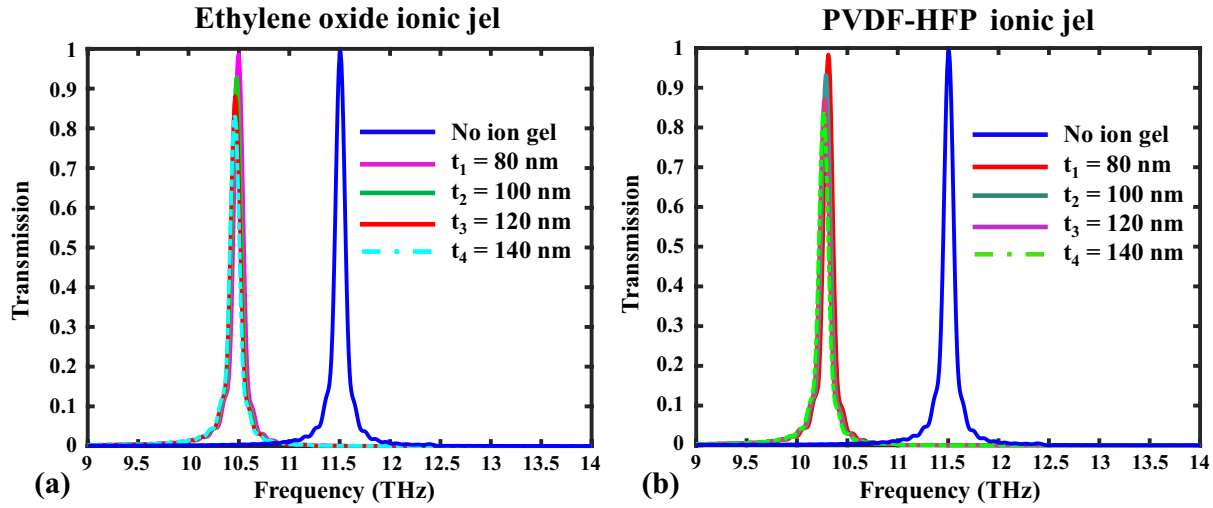

Fig. 7. Transmission spectrum of the filter (**a**) with ethylene oxide ion gel (refractive index 1.359) at different thicknesses, and (**b**) with PVDF-HFP ion gel (refractive index 1.42) at different thicknesses.

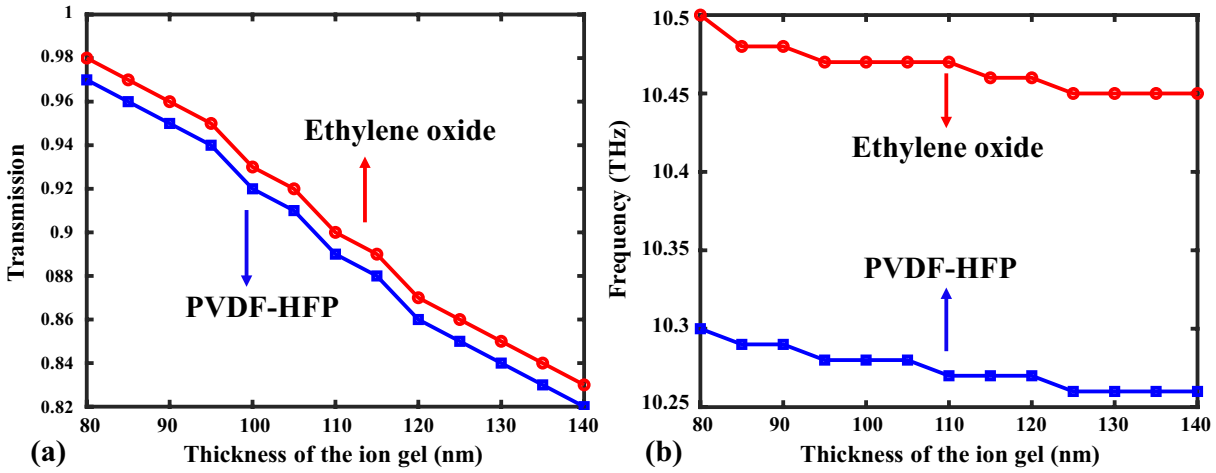

Fig. 8. (**a**) Comparison of filter efficiency for different ion gel thicknesses, and (**b**) comparison of filter frequency for different ion gel thicknesses.

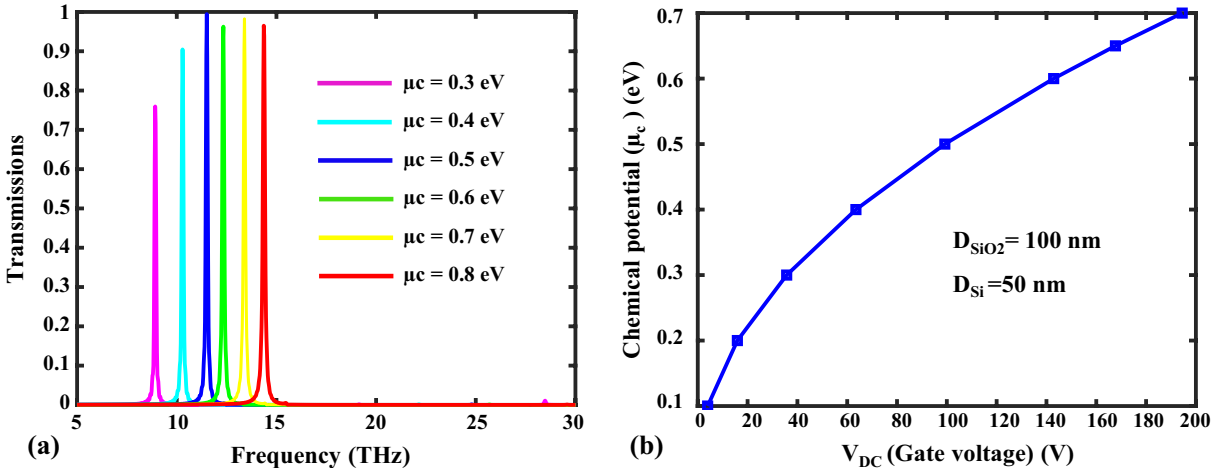

Fig. 9. (**a**) Frequency response of the filter to variations in the chemical potential of graphene. (**b**) Adjusting chemical potential via gate voltage control.

C_{SiO2} and C_{Si} are the capacitances associated with SiO_2 and Si substrates, respectively. Finally, employing Eqs. (4) and (7), we derive the gate voltage Eq. (8) from the following expression[42]:

$$V_{DC} = \left(\frac{e}{\pi c_{ox}}\right) \cdot \left(\frac{\mu_c}{\hbar v_f}\right)^2 \tag{8}$$

Figure 9b depicts the changes in chemical potential achieved through gate voltage adjustment. Frequency changes due to variations in chemical potential occur because, according to Eq. (4), the Fermi energy or chemical potential changes with alterations in bias voltage. According to Eqs. (2) and (3), changes in chemical potential affect the surface conductivity of graphene. As per Eq. (1), changes in the surface conductivity of graphene alter the propagation of electromagnetic waves in GNRs[31].

Analyzing the filter's frequency response by varying the length of the L_3 nanoribbon

The graphene bandpass optical filter detailed in section "Tunable narrow single-mode bandpass filter" constitutes the focal point of this study. As illustrated in Fig. 5a, within the L_3 nanoribbon, the intensity of the electromagnetic field at the resonance frequency significantly surpasses that of other nanoribbons, designating the L_3 nanoribbon as the resonator of this filter. Variations in the dimensions of this nanoribbon directly influence the transmission spectrum's efficacy, frequency, FWHM, and Q-factor of the filter.

In this section, our focus is on attaining the most optimal frequency response by scrutinizing the effects of altering the length of the L_3 nanoribbon, as depicted in Fig. 10a. The length of the L_3 nanoribbon ranged from 40 to 65 nm, with a fixed width and gap of 30 nm. As shown in Fig. 10b,c, the optimal length was found to be 40 nm, yielding a maximum transmission spectrum amplitude of 99%, a Q-factor of 100, and a FWHM of 0.115 THz at the frequency of 11.5 THz.

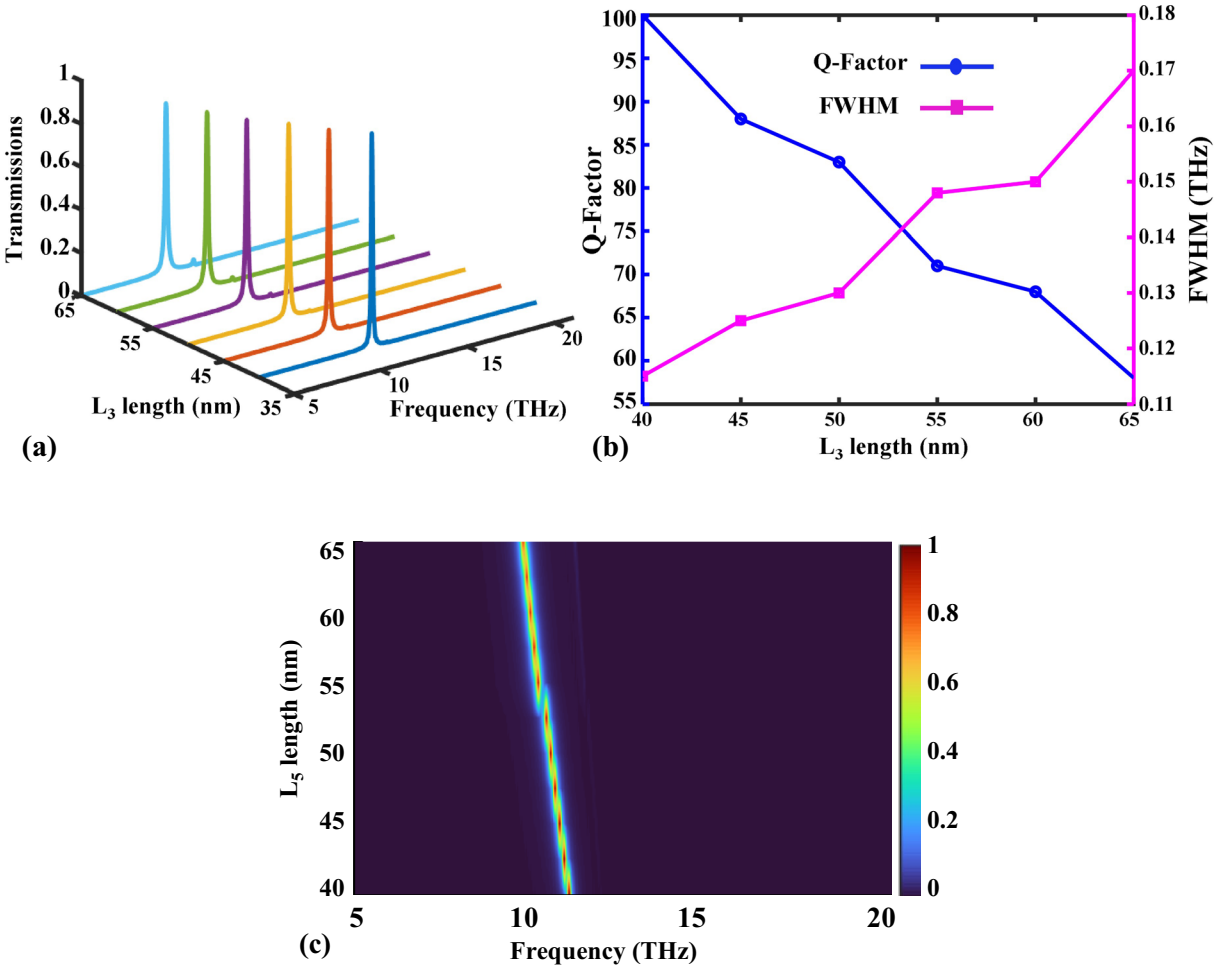

Fig. 10. (**a**) The filter's frequency response to variations in the length of the L_3 nanoribbon, (**b**) alterations in the Q-factor and FWHM with changes in the length of the L_3 nanoribbon, (**c**) various lengths of L_3 nanoribbons corresponding to the resonance frequency of the filter.

Assessing the frequency response of the filter by creating a gap

One approach to eliminate additional harmonics in the frequency response of waveguides and filters is to create gaps in the device structure. However, it's worth noting that the presence of a gap can lead to the narrowing and reduction of the transmission spectrum's efficiency. Depending on the application of the filter, a trade-off between these parameters must be carefully considered. Additionally, determining the optimal position for the gap is crucial. Typically, in filters utilizing GNRs, the most suitable location is between the resonator and the input/output waveguides. In Fig. 11a–d, the impact of gap variations on transmission spectrum efficiency, FWHM, Q-factor, and frequency is examined. The optimal gap width is identified as 30 nm, maintaining a fixed frequency of 11.5 THz.

The impact of variations in the refractive index of the substrate on the filter

The resonance frequency of optical filters is influenced by variations in the refractive index of the substrate. This characteristic finds application in sensors designed to detect substances introduced to the substrate. A sensor's sensitivity correlates with its ability to accurately detect samples on the substrate. Sensitivity is quantified using the following Eq. (9)[43].

$$S = \frac{\Delta fr}{\Delta n}\left(\frac{nm}{RIU}\right) \tag{9}$$

In the Eq. (9) above, Δfr denotes the frequency changes in the resonance frequency, and Δn represents alterations in the refractive index.

In this section, we investigate the alterations in the transmission spectrum of the filter resulting from changes in the refractive index of the SiO_2 substrate. The variations in the transmission spectrum due to changes in the substrate's refractive index are depicted in Fig. 12a,b for Gap = 35 nm, $\mu_c = 0.6$ eV, and Gap = 30 nm, $\mu_c = 0.5$ eV, respectively. According to Fig. 12b, at a Gap of 30 nm and μ_c set at 0.5 eV, with a refractive index of 1.6, the transmission spectrum achieves higher efficiency compared to other refractive indices. The filter's sensitivity

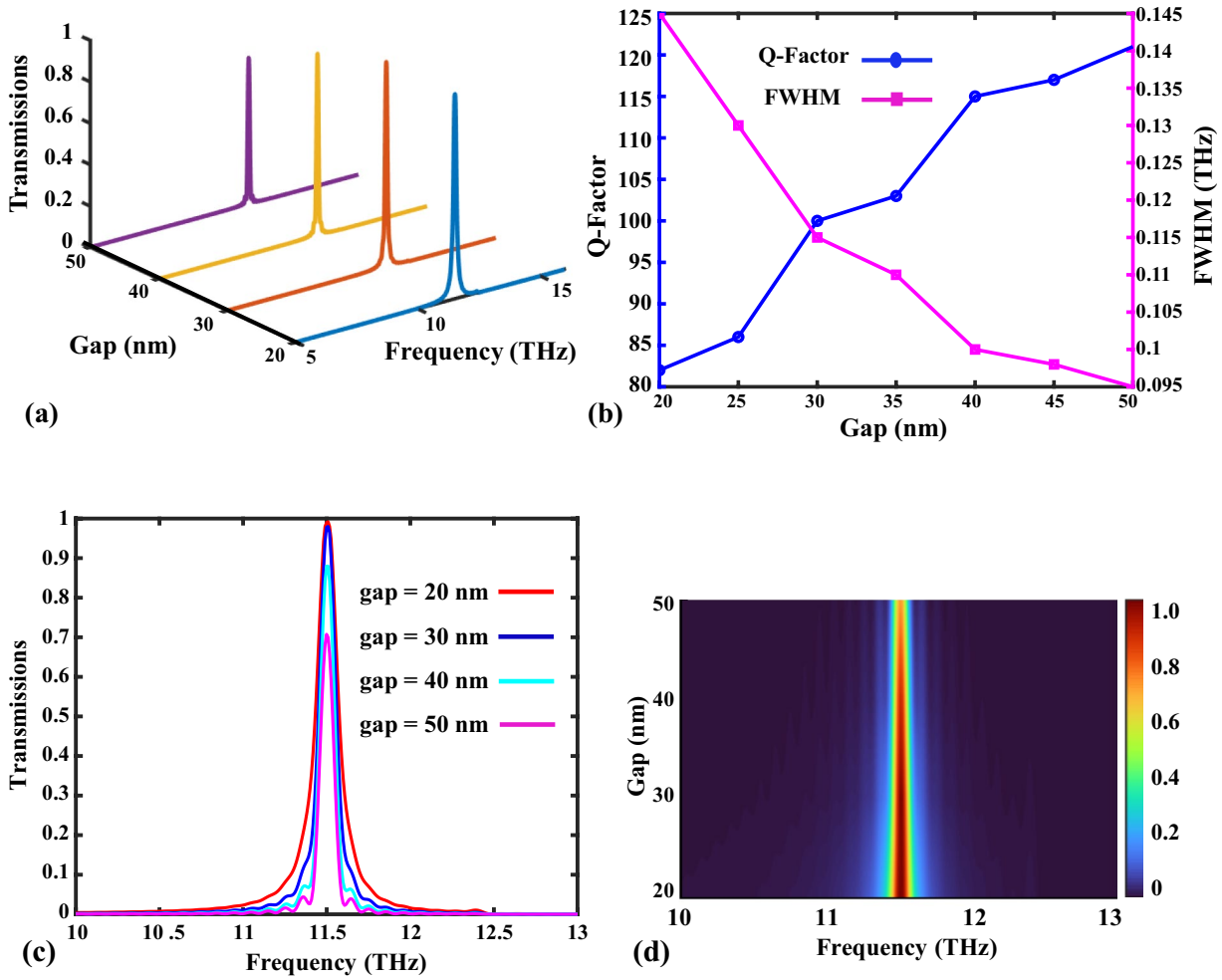

Fig. 11. (**a**) The filter's frequency response to variations in the gap, (**b**) alterations in the Q-factor and FWHM with changes in the gap, (**c**) changes in the filter's transfer spectrum with varying gap widths, (**d**) various gap corresponding to the resonance frequency of the filter.

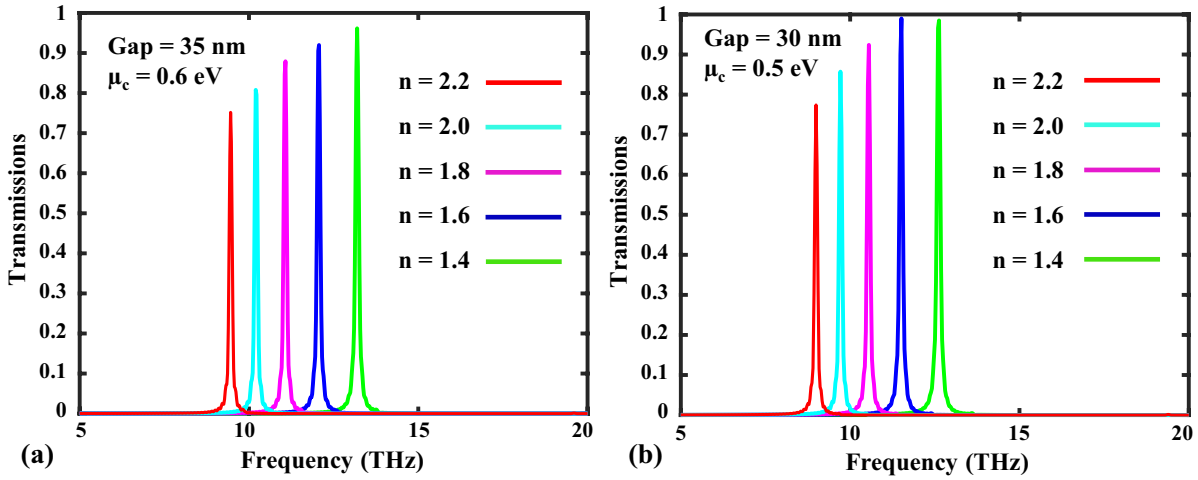

Fig. 12. Variations in the filter's transmission spectrum with alterations in the refractive index of the substrate (**a**) Gap = 35 nm and $\mu_c = 0.6$ eV, (**b**) Gap = 30 nm and $\mu_c = 0.5$ eV.

was calculated using Eq. (9), yielding a value of 4.5 THz/RIU (THz per Refractive Index Unit) and 12,290 nm/RIU (nanometer per Refractive Index Unit).

The characteristics of graphene optical filters, including the number of modes, resonance frequency, transmission spectrum efficiency, Q-factor, and FWHM, have been compared with those outlined in Table 4. Upon examination of the table, it becomes evident that the filter detailed in this paper exhibits the highest transmission spectrum efficiency and the narrowest FWHM value. Furthermore, the Q-factor of the filter ranks one of the highest in this domain.

Fabrication of optical devices consisting of GNRs

Fabricating GNRs with nanometer-scale gaps is highly practical. One conventional method is electron beam lithography. In this method, the sample is first fixed in place, and a rotating electron beam is directed onto it. An etching mask then forms the GNR structure with a specific shape under the electron beam. Finally, the etched area is treated with oxygen plasma to remove the remaining photoresist, creating a GNR on the desired substrate. Additionally, SiO_2, Si, and Au layers can be deposited using conventional chemical vapor deposition methods[31]. Another method to fabricate GNRs on a substrate is nanoparticle etching (NPE). A key advantage of the NPE method is that it preserves the edges of the GNR[24]. To establish connections and apply voltage for adjusting the chemical potential, the top gate method, as explained in Fig. 6, can be used.

Conclusion

In this study, we employed a three-part process to design a narrowband optical filter. The transmission spectrum and electromagnetic field distribution were investigated using the 3D-FDTD and CMT methods. Utilizing GNRs, the filter demonstrated tunability within the 8–14 THz range through the application of a bias voltage. The results

References	Year	Number of modes	Frequency (THz)	Transmission (%)	Q-Factor	FWHM (THz)
[44]	2014	2	16	68	3.7	4.4
[45]	2014	2	32	46	27	1.2
[46]	2015	2	18	76	22.5	0.8
[47]	2017	3	23–29	72	28.8	1.03
[48]	2017	2	14–23	78	25	0.84
[49]	2018	2	13–18	60	33.7	0.48
[50]	2018	1	22–25	70	22	0.5
[51]	2018	3	16–30	96	10.6	1.32
[52]	2018	2	11–20	99	13.5	0.98
[31]	2020	1	40	55	30	1.36
[53]	2021	1	2.4	100	14	0.18
[54]	2022	3	28–40	58	21.51	1.38
[55]	2023	3	27–37	97	100	0.31
[42]	2024	1	10–20	95	107	0.14
This paper	2024	1	8–14	99	100	0.115

Table 4. Comparing the performance of the proposed graphene optical filter with that of other papers.

obtained from the filter designed in section "Tunable narrow single-mode bandpass filter" highlight its exceptional parameters, including high transmission efficiency, a high Q-factor, narrow FWHM, and high sensitivity. Consequently, this filter holds promise for applications in optical integrated circuits, optical communication, and optical measurements within the terahertz range.

Data availability

The datasets and materials used and/or analyzed during the current study are available from the corresponding author on reasonable request (author corresponding: Ali A. Orouji).

Received: 3 May 2024; Accepted: 2 September 2024
Published online: 11 September 2024

References

1. Mohammadi, G., Orouji, A. A. & Danaie, M. A high-performance and high-resolution optical refractive index sensor using a compact photonic crystal ring resonator. *Sens. Imaging* **25**, 1–13 (2024).
2. Tavakoli, M. & Shirpay, A. Investigating the role of structural parameters of gold thin film nanohole arrays on the plasmonic phenomenon of extraordinary optical transmission. *J. Comput. Electron.* **23**, 540–551 (2024).
3. Ramachandran, T., Faruque, M. R. I. & Al-Mugren, K. S. Asymmetric metamaterial sandwich structure with NIM characteristics for THz imaging application. *Sci. Rep.* **14**, 6258 (2024).
4. Wang, Y. *et al.* Catalysis with two-dimensional materials confining single atoms: Concept, design, and applications. *Chem. Rev.* **119**, 1806–1854 (2018).
5. Ullah, Z. *et al.* A review on the development of tunable graphene nanoantennas for terahertz optoelectronic and plasmonic applications. *Sensors* **20**, 1401 (2020).
6. Sgouros, A. P., Kalosakas, G., Papagelis, K. & Galiotis, C. Compressive response and buckling of graphene nanoribbons. *Sci. Rep.* **8**, 9593 (2018).
7. Sharif, M. A. Spatio-temporal modulation instability of surface plasmon polaritons in graphene-dielectric heterostructure. *Physica E Low Dimens. Syst. Nanostruct.* **105**, 174–181 (2019).
8. Udos, W. *et al.* Surface plasmon sensor for lead ion (Pb2+) detection using graphene oxide–Gold coated tilted fiber Bragg grating. *Results Opt.* **12**, 100502 (2023).
9. Najjari, V., Mirzanejhad, S. & Ghadi, A. High-performance plasmonic band-pass/band-stop/cut-off filter using elliptical and rectangular ring resonators. *Results Opt.* **12**, 100495 (2023).
10. Nickpay, M.-R., Danaie, M. & Shahzadi, A. Graphene-based metamaterial absorber for refractive index sensing applications in terahertz band. *Diam. Relat. Mater.* **130**, 109539 (2022).
11. Sharifi, H., Pourziad, A. & Bemani, M. Nano optical temperature sensor based on fiber Bragg grating using graphene. *Results Opt.* **9**, 100318 (2022).
12. De Carvalho, M. M., de Souza, E. A. T. & Saito, L. A. M. Graphene-based PAM-4 modulator compatible with CMOS platform operating over DWDM C-Band. *Results Opt.* **5**, 100110 (2021).
13. Qiu, C. *et al.* All-optical control of light on a graphene-on-silicon nitride chip using thermo-optic effect. *Sci. Rep.* **7**, 17046 (2017).
14. Ahmadkhani, S. *et al.* Multiband flattening and linear Dirac band structure in graphene with impurities. *Phys. Rev. B* **107**, 075401 (2023).
15. Korani, N. & Danaie, M. A plasmonic terahertz perfect absorber based on L-shaped graphene patches and gold rods. *Appl. Phys. A* **129**, 806 (2023).
16. Naghizade, S. & Saghaei, H. Tunable graphene-on-insulator band-stop filter at the mid-infrared region. *Opt. Quantum Electron.* **52**, 1–13 (2020).
17. Yildirim, D. U., Ghobadi, A. & Ozbay, E. Near-absolute polarization insensitivity in graphene based ultra-narrowband perfect visible light absorber. *Sci. Rep.* **8**, 15210 (2018).
18. Ram, G. C., Sambaiah, P., Yuvaraj, S. & Kartikeyan, M. V. Graphene based filter design using triangular patch resonator for THz applications. *Nano Commun. Netw.* **38**, 100477 (2023).
19. Chen, J. *et al.* High-selectivity bandpass filter with controllable attenuation based on graphene nanoplates. *Materials* **15**, 1694 (2022).
20. Xing, P., Ooi, K. J. A. & Tan, D. T. H. Ultra-broadband and compact graphene-on-silicon integrated waveguide mode filters. *Sci. Rep.* **8**, 9874 (2018).
21. Wang, D. *et al.* Twisted bilayer zigzag-graphene nanoribbon junctions with tunable edge states. *Nat. Commun.* **14**, 1018 (2023).
22. Sepahvandi, V., Rezaei, B. & Aly, A. H. Tunable multichannel Fibonacci one-dimensional terahertz photonic crystal filter. *Sci. Rep.* **13**, 5631 (2023).
23. Gezimati, M. & Singh, G. Terahertz imaging and sensing for healthcare: Current status and future perspectives. *IEEE Access* **11**, 18590–18619 (2023).
24. Mohammadi, G., Orouji, A. & Danaie, M. Highly compact tunable hourglass-shaped graphene band-stop filter at terahertz frequencies. *Results Opt.* **13**, 100575 (2023).
25. Hanson, G. W. Dyadic Green's functions and guided surface waves for a surface conductivity model of graphene. *J. Appl. Phys.* **103**, 064302 (2008).
26. Wu, D., Tian, J., Li, L. & Yang, R. Plasmon induced transparency and refractive index sensing in a new type of graphene-based plasmonic waveguide. *Opt. Commun.* **412**, 41–48 (2018).
27. Liang, X.-Y., Ding, N., Ng, S.-P. & Wu, C.-M.L. Adsorption of gas molecules on Ga-doped graphene and effect of applied electric field: A DFT study. *Appl. Surf. Sci.* **411**, 11–17 (2017).
28. Xu, B., Gu, C., Li, Z. & Niu, Z. A novel structure for tunable terahertz absorber based on graphene. *Opt. Express* **21**, 23803–23811 (2013).
29. Xu, K. *et al.* Direct measurement of Dirac point energy at the graphene/oxide interface. *Nano Lett.* **13**, 131–136 (2013).
30. Wang, R. *et al.* Control of carrier type and density in exfoliated graphene by interface engineering. *ACS Nano* **5**, 408–412 (2011).
31. Asgari, S. & Fabritius, T. Tunable mid-infrared graphene plasmonic cross-shaped resonator for demultiplexing application. *Appl. Sci.* **10**, 1193 (2020).
32. Li, Q., Wang, T., Su, Y., Yan, M. & Qiu, M. Coupled mode theory analysis of mode-splitting in coupled cavity system. *Opt. Express* **18**, 8367–8382 (2010).
33. Razani, A. N., Rezaei, P., Zamzam, P., Khatami, S. A. & Daraei, O. M. Absorption-based ultra-sensitive RI sensor based on the flower-shaped graphene resonator for early detection of cancer. *Opt. Commun.* **524**, 128775 (2022).
34. Liu, A., Wolf, P., Schulze, J.-H. & Bimberg, D. Fabrication and characterization of integrable GaAs-based high-contrast grating reflector and Fabry-Pérot filter array with GaInP sacrificial layer. *IEEE Photon. J.* **8**, 1–9 (2016).

35. Khatami, S. A., Rezaei, P. & Danaie, M. High accuracy graphene-based refractive index sensor: Analytical approach. *Diam. Relat. Mater.* **2024**, 111225 (2024).
36. Kim, J. T., Choi, H., Choi, Y. & Cho, J. H. Ion-gel-gated graphene optical modulator with hysteretic behavior. *ACS Appl. Mater. Interfaces* **10**, 1836–1845 (2018).
37. Wang, D. *et al.* Recent advanced applications of ion-gel in ionic-gated transistor. *Npj Flexible Electron.* **5**, 13 (2021).
38. Lee, K. H. *et al.* 'Cut and stick' rubbery ion gels as high capacitance gate dielectrics. *Adv. Mater.* **24**, 4457–4462 (2012).
39. Lee, J., Panzer, M. J., He, Y., Lodge, T. P. & Frisbie, C. D. Ion gel gated polymer thin-film transistors. *J. Am. Chem. Soc.* **129**, 4532–4533 (2007).
40. Feng, Y., Liu, Y., Shi, Y., Wang, X. & Dong, D. An ultra-compact tunable intersection structure based on graphene nanoribbon. *J. Phys. D Appl. Phys.* **50**, 185101 (2017).
41. Armaghani, S., Khani, S. & Danaie, M. Design of all-optical graphene switches based on a Mach–Zehnder interferometer employing optical Kerr effect. *Superlatt. Microstruct.* **135**, 106244 (2019).
42. Mohammadi, G., Orouji, A. A. & Danaie, M. Highly selective single-mode graphene bandpass filter based on Wilkinson power divider structure. *Diam. Relat. Mater.* **2024**, 111141 (2024).
43. Nohoji, A. H. A. & Danaie, M. Highly sensitive refractive index sensor based on photonic crystal ring resonators nested in a Mach–Zehnder interferometer. *Opt. Quantum Electron.* **54**, 574 (2022).
44. Wang, J., Lu, W. B., Li, X. B., Ni, Z. H. & Qiu, T. Graphene plasmon guided along a nanoribbon coupled with a nanoring. *J. Phys. D Appl. Phys.* **47**, 135106 (2014).
45. Li, H.-J., Wang, L.-L., Sun, B., Huang, Z.-R. & Zhai, X. Tunable mid-infrared plasmonic band-pass filter based on a single graphene sheet with cavities. *J. Appl. Phys.* **116**, 224505 (2014).
46. Zhuang, H., Kong, F., Li, K. & Sheng, S. Plasmonic bandpass filter based on graphene nanoribbon. *Appl. Opt.* **54**, 2558–2564 (2015).
47. Janfaza, M., Mansouri-Birjandi, M. A. & Tavousi, A. Tunable plasmonic band-pass filter based on Fabry–Perot graphene nanoribbons. *Appl. Phys. B* **123**, 1–9 (2017).
48. Su, W. & Chen, B. Graphene-based tunable terahertz filter with rectangular ring resonator containing double narrow gaps. *Pramana* **89**, 1–5 (2017).
49. Dolatabady, A., Asgari, S. & Granpayeh, N. Tunable mid-infrared nanoscale graphene-based refractive index sensor. *IEEE Sens. J.* **18**, 569–574 (2017).
50. Zhou, D., Wang, X., Zhu, H. & Shen, F. Graphene-based tunable multichannel filter with arithmetic sequence quasiperiodic structure. *Optik (Stuttg)* **174**, 282–288 (2018).
51. Tavousi, A., Mansouri-Birjandi, M. A. & Janfaza, M. Optoelectronic application of graphene nanoribbon for mid-infrared bandpass filtering. *Appl. Opt.* **57**, 5800–5805 (2018).
52. Su, W. A four-port ultra-compact terahertz splitting filter based on graphene nanoribbon. *IEEE Photon. Technol. Lett.* **31**, 86–89 (2018).
53. Belhadj, W. & Al-Ahmadi, A. N. Tunable narrowband terahertz multichannel filter based on one-dimensional graphene-dielectric photonic crystal. *Opt. Quantum Electron.* **53**, 1–17 (2021).
54. Janfaza, M., Mansouri-Birjandi, M. A. & Tavousi, A. Applications of tunable mid-infrared plasmonic square-nanoring resonator based on graphene nanoribbon. *Plasmonics* **17**, 479–490 (2022).
55. Davoudi, I., Ghayour, R. & Barati, R. Tunable plasmonic terahertz filter based on a suspended monolayer graphene on a ring resonator. *Opt. Quantum Electron.* **55**, 218 (2023).

Acknowledgements

The authors sincerely appreciate the valuable considerations and comments provided by the respected reviewers, which have significantly enhanced the scientific quality of this paper.

Author contributions

Ghader Mohammadi: Design, analysis, and investigation, writing-original draft. Ali Asghar Orouji: Supervision, writing-reviewing and editing. Mohammad Danaie: Supervision, writing-reviewing and editing.

Competing interests

The authors declare no competing interests.

Ethical approval

We the undersigned that the manuscript entitled "A Tunable Narrow Single-Mode Bandpass Filter Using GNRs for THz Applications" is original, has not been thoroughly or partly published before, and is not currently being considered for publication elsewhere. Also, results are presented honestly, and without fabrication, falsification, or inappropriate data manipulation. We confirm that the manuscript has been read and approved by all named authors and that there are no other persons who satisfied the criteria for authorship but are not listed. We further confirm that all have agreed with the order of authors listed in the manuscript of us.

Declaration of generative AI in scientific writing

Authors have used these technologies to improve readability and language.

Additional information

Correspondence and requests for materials should be addressed to A.O.